Available online at www.sciencedirect.com
ScienceDirect
Nuclear Physics B Proceedings Supplement 00 (2014) 1–6
Nuclear Physics B Proceedings Supplement

Matteo Sani on behalf of the CMS Collaboration

University of California, San Diego
9500 Gilmann Dr, La Jolla CA 92093, United States

Abstract

Using the high mass resolution channels $H \to \gamma\gamma$ and $H \to ZZ^* \to 4\ell$, where the leptons are electrons or muons, a precise measurement of the Higgs boson mass is obtained. The analysis is based on pp collision data collected at centre-of-mass energies of 7 and 8 TeV, corresponding to integrated luminosities of 5 fb^{-1} and 19.7 fb^{-1}, respectively. The results, together with the strategy of the measurement and the methods to control the main systematic errors on the energy and momentum scale, are discussed in detail.

Keywords: LHC, CMS, Higgs boson, mass

1. Introduction

Since the CMS Collaboration announced its discovery in 2012 [1], the effort has been focused in measuring the properties of the Higgs boson. Among the various parameters, the mass of the newly discovered particle (m_H) is of particular interest since its value is not predicted by the Standard Model (SM). Moreover SM predictions are fully determined once the mass of the boson has been measured and knowing the value of m_H allows to over-constraint the global electroweak fit to test its self consistency and possible hints of new physics.

In the following the results of the Higgs boson mass measurement performed with the CMS detector [2] are presented. The analysis is based on the pp collision data collected at centre-of-mass energies of 7 and 8 TeV, corresponding to integrated luminosities of 5.1 fb^{-1} and 19.7 fb^{-1}, respectively. The strategy of the measurement and the methods to control the main systematic errors on the energy and momentum scale are discussed in detail. In this measurement only the two best mass resolution channels are considered: $H \to \gamma\gamma$ and $H \to ZZ^* \to 4\ell$.

The $H \to \gamma\gamma$ analysis [3] measures a narrow signal mass peak over a smoothly falling background due to events originating from prompt non-resonant diphoton production or from events with at least one jet misidentified as an isolated photon. The sample of events with a photon pair is split into mutually exclusive event classes targeting different production processes (gluon fusion, VBF, VH and $t\bar{t}H$). The remaining *untagged* events are subdivided into different classes based on the output of an multivariate classifier that assigns a high score to signal-like events and to events with a good mass resolution.

The $H \to ZZ^* \to 4\ell$ analysis [4] measures a four-lepton mass peak over a small continuum background. The dominant irreducible background in this channel is due to non-resonant $ZZ^{(*)}$ production with both Z bosons decaying to a pair of charged leptons and is estimated from simulation. The smaller reducible backgrounds with misidentified leptons, mainly from the production of Z + jets, $t\bar{t}$, and WZ + jets, are estimated from data. To increase the sensitivity to the production mechanism, the event sample is split into two categories based on jet multiplicity.

2. Lepton and Photon Momentum Scale and Resolution

2.1. Leptons

To obtain a precise measurement of the mass of a resonance decaying into four leptons, it is crucial to calibrate the individual lepton momentum scale and resolution to a level such that the systematic uncertainty in the

measured value of m_H is substantially smaller than the statistical uncertainty in the current dataset.

The electron reconstruction combines information from the ECAL and the tracker [5]. The energy of the ECAL clusters is corrected for the imperfect containment, the electron energy not deposited in the ECAL and leakage arising from showers near gaps between crystals or between ECAL modules. This is done using a regression technique based on boosted decision trees (BDT) [6] trained on a simulated dielectron sample with the pileup conditions equivalent to the ones measured on data. Using such a multivariate technique improves the effective width of the reconstructed invariant mass by 25% compared to that obtained with a more traditional approach based on ECAL-only energy measurements and corrections with a parameterized energy response obtained from simulation.

The precision of the electron momentum measurement is dominated by the ECAL at high energies, whereas for low-p_T electrons the precision is dominated by the tracker momentum determination. However, for electrons near poorly instrumented regions, such as the crack between the EB and the EE, the intermodule cracks, or regions close to dead channels, the measurement accuracy and resolution can also be improved by combining the ECAL energy with the track momentum. Hence the magnitude of the electron momentum is determined by combining the two estimates and their uncertainties with a multivariate regression function while the electron direction is taken from the fitted track parameters at the point of closest approach to the nominal beam spot position.

Muon reconstruction combines information from both the Silicon Tracker and the Muon System. The matching between track segments from the two detectors is done either outside-in (i.e. starting from a track in the muon system) or inside-out (i.e. starting from a track in the Silicon Tracker) [7].

The p_T resolution for muons in the momentum range 5 to 100 GeV varies between 1.3% and 2.0% in the barrel, and up to 6% in the endcaps. The dominant effect determining the resolution is the multiple scattering of muons in the tracker material. The accuracy of the hit measurements in the muon chambers and the overall detector alignment contribute to a lesser degree to the momentum measurement. This is achieved using several alignment procedures using cosmic muons, optical surveys, a laser system, and, finally, Z events.

2.2. Lepton Calibration

The determination of the momentum differs for electrons and muons, and it depends on the different CMS subdetectors involved in their reconstruction. The CMS simulation is based on Geant4 [8] and the best knowledge of the detector conditions is encoded in the ECAL calibrations and tracker and muon system alignment. Nevertheless, small discrepancies between data and simulation remain. In the case of the electron momentum scale and resolution, the main sources of discrepancy are the residual tracker misalignment and the imperfect corrections at the crystal level of the transparency loss due to irradiation (reduced to a negligible level after the calibrations). In case of muons, the momentum determination is affected by the tracker and muon system alignment geometry used for the reconstruction. The momentum scale and resolution for electrons and muons are studied using different data control samples for different p_T^{ℓ} ranges such as the dileptons from decays of the J/ψ, Υ (nS) (only for muons) and Z resonances.

For electrons, the calibration procedure consists of three steps. First, a set of time dependent corrections for the momentum scale is obtained by comparing the displacement of the peak position in the distributions of the Z-boson mass in the data and in the simulation in different pseudorapidity regions and in two categories depending on the amount of bremsstrahlung. Then a linearity correction to the momentum scale is applied, in data and in simulated Z→ee events, to account for the p_T-dependent differences between data and simulation by comparing the dielectron mass distributions, binned in p_T^{e} of one of the two electrons. Finally the energies of single electrons in the simulation are smeared by applying a Gaussian multiplicative factor in order to achieve the resolution observed in the data Z-boson sample. The electron relative momentum scale between data and simulation is consistent within 0.2% in the central barrel and up to 0.3% in the forward part of the ECAL endcaps. σ_{eff} ranges from 1.2% to 4% according to electron quality category and the relative difference between data and simulation is less than 3%.

For muons, an absolute measurement of momentum scale and resolution is performed by using a reference model of the Z line shape convolved with a Gaussian function. The bias in the reconstructed muon p_T is determined from the position of the Z mass peak as a function of muon kinematic variables, and is corrected for the data accordingly. A correction for the resolution is also derived for the simulation from a fit to the Z→ $\mu\mu$ and other low-mass dimuon resonances mass spectra. The agreement between the observed and simulated mass scales is within 0.1% in the entire pseudorapidity range of interest. In the whole kinematic range considered for this analysis, the instrumental Z-peak mass resolution

observed in data is consistent with that in the simulation within about 5%, see Figure 1.

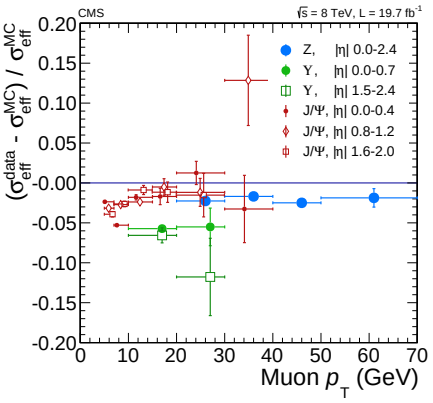

Figure 1: Relative difference between the dimuon mass resolutions in data and simulation as measured from J/ψ, Υ(nS) and Z decays as a function of the average muon p_T^{μ}.

2.3. Photons

Photon candidates are reconstructed from energy deposits in the ECAL using algorithms that constrain the clusters in η and ϕ to the shapes expected from electrons and photons with high p_T [9]. The algorithms do not make any hypothesis as to whether the particle originating from the interaction point is a photon or an electron; when reconstructed in this way, electrons from $Z \to ee$ events provide measurements of the photon trigger, reconstruction, and identification efficiencies, and of the photon energy scale and resolution.

Photon energy is computed from the signals recorded by the ECAL. In the region covered by the preshower detector ($|\eta| > 1.65$) the signals recorded in it are also considered. In order to obtain the best energy resolution, the calorimeter signals are calibrated and corrected for several detector effects (e.g. variation of crystal transparency). The single-channel response of the ECAL is equalized exploiting the phi-symmetry of the energy flow, the mass constraint on the energy of the two photons in π^0 and η decays and the momentum constraint on the energy of isolated electrons from W and Z-boson decays. Finally, the containment of the shower in the clustered crystals, the shower losses for photons that convert in the material upstream of the calorimeter, and the effects of pileup, are corrected using a multivariate regression technique. The regression provides a per-photon estimate of the ratio of true energy to uncorrected cluster energy. The most probable value of this distribution is taken as the corrected photon energy. The width of the Gaussian core is further used as a per-photon estimator of the energy uncertainty.

2.4. Photon Calibration

A multistep procedure has been implemented to correct the energy scale in data and to determine the parameters of Gaussian smearing to be applied to showers in simulated events so as to reproduce the energy resolution seen in data. The energy scale in data is equalized with that in simulated events and residual long-term drifts in the response are corrected, using $Z \to ee$ decays in which the electron showers are reconstructed as photons. Following this, the photon energy resolution predicted by the simulation is made more realistic by adding a Gaussian smearing determined from the comparison between the $Z \to ee$ line-shape in data and in simulated events. The amount of smearing required is extracted differentially in pseudorapidity and R9 (cluster shape variable used to discriminate converted and unconverted photons). In the fits from which the required amount of smearing is extracted, the data energy scale is allowed to float, and a residual scale correction for the data is extracted in the same bins. A sufficient number of $Z \to ee$ events is available in the 8 TeV data to allow a third step, in which the energy scale for the ECAL barrel is further corrected in bins defined by ranges in $|\eta|$, R9, and E_T, and the smearing magnitude is allowed to have an energy dependence. Figure 2 shows the invariant mass of electron pairs reconstructed in $Z \to ee$ events in the 8 TeV data and in simulated events in which the electron showers are reconstructed as photons, and the full set of corrections to the data, and smearing of the simulated energies, are applied. The selection applied to the diphoton candidates is the same, apart from the inversion of the electron veto, as is applied to diphoton candidates entering the $H \to \gamma\gamma$ analysis. There is excellent agreement between the data and the simulation in the core of the distributions. A slight discrepancy is present in the low-mass tail in the endcaps, where the Gaussian smearing is not enough to account for some noticeable non-Gaussian energy loss. The mass peaks are shifted from the true Z-boson mass, both in data and simulation, because the electron showers are reconstructed as photons.

3. Higgs Boson Mass Measurement

3.1. $H \to ZZ^* \to 4\ell$

In order to measure the mass of the Higgs boson precisely and to correctly assign the uncertainties in this

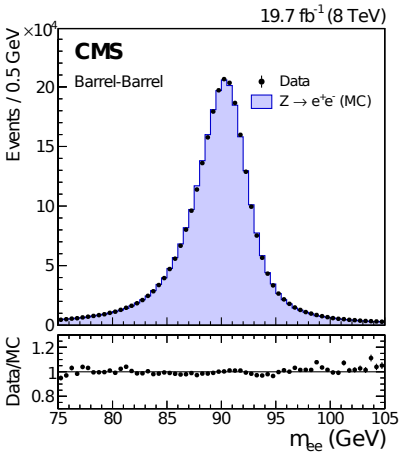

Figure 2: Invariant mass of e^+e^- pairs in $Z \to ee$ events in the 8 TeV data (points), and in simulated events (histogram), in which the electron showers are reconstructed as photons, and the full set of photon corrections and smearing are applied. The comparison is shown for events with both showers in the barrel. For each bin, the ratio of the number of events in data to the number of simulated events is shown in the lower plot.

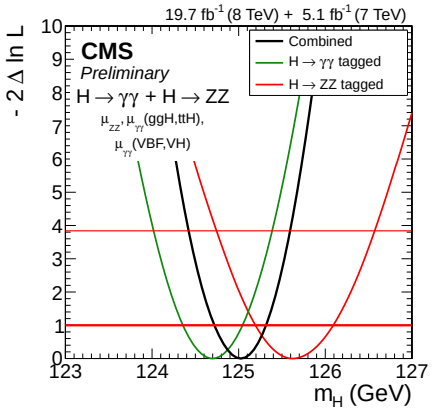

Figure 3: Scan of the negative log likelihood versus the SM Higgs boson mass m_H, for each of the three channels separately and the combination of the three, where the dashed line represents the scan including only statistical uncertainties.

measurement, the four-lepton mass uncertainties estimated on a per-event basis, are incorporated into the likelihood. An event-by-event estimator of the mass resolution is built from the single-lepton momentum resolutions evaluated from the study of a large number of J/ψ and $Z \to \ell\ell$ data events. The relative mass resolution ($\sigma_{m_{4\ell}}/m_{4\ell}$) is then used together with $m_{4\ell}$ and D_{kin} (a discriminant, including the observed kinematics that uniquely define the four-lepton configuration in the center-of-mass frame).

Figure 3.1 shows the profile likelihood scan versus the SM Higgs boson mass for the single channels, combining 7 and 8 TeV data and for the combination of all the channels. The Higgs boson cross section is left floating in the fit. The measured mass is $m_H = 125.6 \pm 0.4(\text{stat}) \pm 0.2(\text{syst})$ GeV. To decompose the total mass uncertainty into statistical and systematic components, a fit with all nuisance parameters fixed at their best-fit values is performed.

For electrons, a p_T^e dependence of the momentum scale is observed, but it only marginally affects the four-lepton mass, and the per-electron uncertainty is propagated, accounting for the correlations, to the 4e and 2e2μ channels. This dependence is corrected for, but the observed deviation is conservatively used as a systematic uncertainty, resulting in effects of 0.3% and 0.1% on the mass scales of the two channels, respectively. The systematic uncertainty in the muon momentum scale translates into a 0.1% uncertainty in the 4μ mass scale. The effect of the energy resolution uncertainties is taken into account by introducing conservatively a 20% uncertainty in the simulated width of the signal mass peak, according to the agreement between per-event estimated and observed mass resolutions in the $Z \to \ell\ell$ events. Shape systematics in the probability density functions used as signal and background models and normalization systematics due to acceptance and efficiency uncertainty are also considered.

3.2. $H \to \gamma\gamma$

The four main Higgs boson production mechanisms can be associated with either fermion couplings (ggH and $t\bar{t}H$) or vector boson couplings (VBF and VH). To make the measurement of the mass of the observed resonance less model dependent the signal strengths of the production processes involving the Higgs boson coupling to fermions and the production processes involving the coupling to vector bosons, are allowed to vary independently. The resulting scan of the negative-log-likelihood ratio, as a function of the mass hypothesis, shown in Figure 3.2, gives a mass of the observed boson as $m_H = 124.70 \pm 0.34$ GeV.

The uncertainty in the measured mass can be separated into statistical and systematic contributions: $m_H = 124.70 \pm 0.31(\text{stat}) \pm 0.15(\text{syst})$ GeV.

Systematic uncertainties from theory play a negligible role while the most important contributions come from uncertainties related to the photon energy scale. The largest contribution is due to the imperfect modeling of the difference between electrons and photons by the MC simulation. The most important cause of which is an imperfect description of the material between the

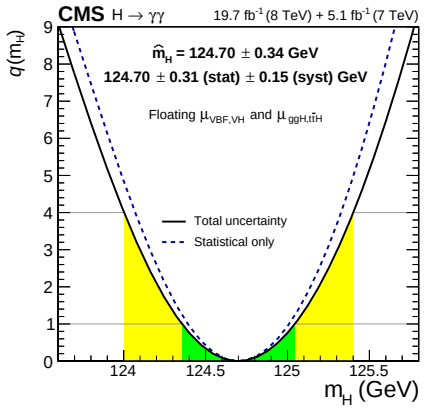

Figure 4: Scan of the likelihood ratio as a function of the hypothesized mass when μ(ggH,t$\bar{\text{t}}$H) and μ(VBF, VH) are allowed to vary independently.

interaction point and the ECAL. Studies of electron bremsstrahlung, photon conversion vertices, and the multiple scattering of pions suggest a deficit of material in the simulation. Although the deficit is almost certainly in specific structures and localized regions, and this hypothesis is supported by the studies, the data/MC discrepancies are slightly smaller than what would be caused by a 10% uniform deficit of material in the region $|\eta| < 1.0$ and a 20% uniform deficit for $|\eta| > 1.0$. The resulting uncertainty in the energy scale has been assessed using simulated samples in which the tracker material is increased uniformly by 10 and 20%, and an uncertainty, with differing magnitude in pseudorapidity and R9 bins, is assigned to photon energies. The systematic uncertainty in the energy scale ranges from 0.03% in the central ECAL barrel up to 0.3% in the outer endcap. Two nuisance parameters are introduced to model this uncertainty, which is fully correlated between the 7 and 8 TeV datasets.

Another discrepancy between data and simulation, relevant to electron-photon differences, is the modeling of the varying fraction of scintillation light reaching the photodetector as a function of the longitudinal depth in the crystal at which it was emitted. Ensuring adequate uniformity was a major accomplishment in the lead tungstate crystal development that was achieved by depolishing one face of each barrel crystal, but an uncertainty in the degree of uniformity achieved remains. In addition, the uniformity is modified by the radiation-induced loss of transparency of the crystals. The effect of the uncertainty, including the effect of radiation-induced transparency loss, has been simulated. It results in a difference in the energy scale between electrons and unconverted photons which is not present in the standard simulation. The magnitude of the uncertainty in the photon energy scale is 0.04% for unconverted photons and 0.06% for converted ones, but the signs of the energy shifts are opposed, and the two anti-correlated uncertainties result in an uncertainty about 0.015% in the mass scale. A further small uncertainty is added to account for imperfect electromagnetic shower simulation. A simulation made with an improved shower description, using the Seltzer - Berger model [10] for the bremsstrahlung energy spectrum, changes the energy scale for both electrons and photons. The much smaller changes in the difference between the electron and photon energy scales, although mostly consistent with zero, are interpreted as a limitation on our knowledge of the correct simulation of the showers, leading to a further uncertainty of 0.05%.

Possible differences between MC simulation and data in the extrapolation from shower energies typical of electrons from $Z \to ee$ decays, to those typical of photons from $H \to \gamma\gamma$ decays, have been investigated with $Z \to ee$ data samples by binning the events according to the scalar sum of the E_T of the two electron showers, and by studying electron showers in $W \to e\nu$ events in which the electron p_T is also measured by the tracker. The effect of the differential nonlinearity in the measurement of photon energies has an effect of up to 0.1% on the diphoton mass scale for diphoton masses close to 125 GeV. In the best untagged event class, in which the diphoton transverse momentum is particularly high, the effect is up to 0.2%. The uncertainties are not completely correlated between the 7 and 8 TeV datasets, since the energy response regression, which would be strongly implicated in any nonlinearity, uses independent sets of regression weights for the two datasets. Moreover, E_T-dependent scale corrections have been applied at 8 TeV for barrel photons, while the corrections at 7 TeV are not E_T-dependent. Studies suggest that there may be as much as 20% correlation between the uncertainties in the energy scale nonlinearities in the 7 and 8 TeV datasets, and this correlation is included in the implementation of the uncertainties.

The energy scale and resolution in data are measured with electrons from $Z \to ee$ decays. The statistical uncertainties in the measurements are small, but the methodology, gives rise to a number of systematic uncertainties related to the imperfect agreement between data and MC simulation. These are estimated and accounted for in the same bins as are used to derive the scale corrections and the resolution smearing for simulated events. The uncertainties range from 0.05% for unconverted photons in the ECAL central barrel, to 0.1% for converted photons in the ECAL outer endcaps.

In addition, for the barrel region, the uncertainty in the energy dependence of the Gaussian smearing applied to the simulation, is also accounted for.

Additional sources of uncertainty that have been investigated and found to be negligible are a possible bias related to the choice of background parameterization, which has been studied using pseudo-experiments where the effect is found to be less than 10 MeV; the effect of the switch of preamplifier when very large signals, E > 200 GeV in the barrel and E_T > 80 GeV in the endcaps, are digitized using a preamplifier with lower gain; and the imperfect simulation of the effect of signals from interactions in previous bunch crossings.

3.3. Higgs Mass Combination

The results of the two analysis previously described are finally combined together [11]. The combined mass is measured to be m_H = 125.03 ± 0.29 GeV. Figure 3.3 shows the scan of the test statistic as a function of the mass (m_H) separately for the two channels and for their combination. The intersections of the curves with the thick horizontal line at 1.00 and thin line at 3.84 define the 68% and 95% CL intervals for the mass of the observed particle, respectively.

To quantify the compatibility of the two individual measurements with each other, a scan of the test statistic has been performed, as a function of the difference between the two mass measurements. The result is $m_{\gamma\gamma}$-$m_{4\ell}$ = −0.87 ± 0.54 GeV; the two measurements agree at the 1.6σ level. The statistical component of the overall uncertainty is evaluated with a likelihood scan fixing all nuisance parameters to their best-fit values. The systematic uncertainty is derived by assuming that the total uncertainty is the sum in quadrature of the statistical and systematic components; the full result can be written as m_H = 125.03 ± 0.26(stat.) ± 0.13(syst.) GeV. To assess the dependency of the mass measurement on the SM Higgs boson hypothesis, the measurement is repeated using the same channels, but with the following two sets of assumptions: allowing a common signal strength modifier to float and constraining the relative production cross sections and branching fractions to the SM predictions, i.e., μ = 1. The results from these two alternative measurements differ by less than 0.1 GeV with respect to the main result, both in terms of the best-fit value and the uncertainties.

4. Summary

Using the high mass resolution channels H → $\gamma\gamma$ and H → ZZ^* → 4ℓ, where the leptons are electrons or muons, a precise measurement of the Higgs boson mass is obtained. The analysis is based on pp collision data collected at centre-of-mass energies of 7 and 8 TeV, corresponding to integrated luminosities of 5 fb^{-1} and 19.7 fb^{-1}, respectively. The mass of the Higgs boson is measured to be m_H = 125.03 ± 0.26(stat) ± 0.13(syst) GeV.

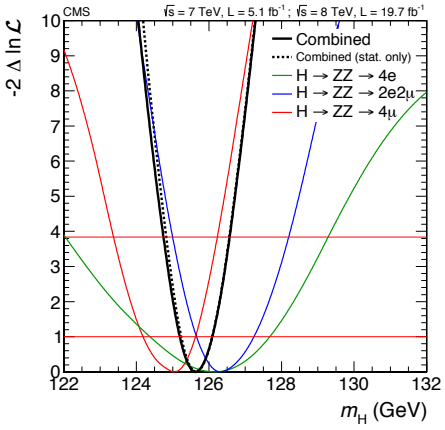

Figure 5: Scan of the test statistic q(m_H) versus the boson mass m_H for the H → $\gamma\gamma$ (green) and 4ℓ (red) final states separately and for their combination (black).

References

[1] CMS Collaboration, Observation of a new boson with mass near 125 GeV in pp collisions at $\sqrt{s}$ =7 and 8 TeV, JHEP 06 (2013) 081.

[2] CMS Collaboration, The CMS experiment at the CERN LHC, JINST 8 (2013) P09009.

[3] CMS Collaboration, Observation of the diphoton decay of the Higgs boson and measurement of its properties, arXiv:1407.0558.

[4] CMS Collaboration, Measurement of the properties of a Higgs boson in the four-lepton final state, arXiv:1312:5353.

[5] CMS Collaboration, Electron reconstruction and identification at $\sqrt{s}$ = 7 TeV, CMS-PAS-EGM-10-004.

[6] P. Speckmayer, A. Hcker, J. Stelzer, H. Voss, The toolkit for multivariate data analysis, TMVA 4, Journal of Physics: Conference Series 219 (3) (2010) 032057.

[7] CMS Collaboration, Performance of CMS muon reconstruction in pp collision events at $\sqrt{s}$ = 7 TeV, JINST 7 (2012) P10002.

[8] GEANT Collaboration, Geant4 - a simulation toolkit, Nucl. Instrum. Meth. A 506 (2003) 250.

[9] CMS Collaboration, Performance and operation of the CMS electromagnetic calorimeter, doi:10.1088/1748-0221/5/03/T03010.

[10] S. Seltzer and M. Berger, Transmission and reflection of electrons by foils, Nucl. Instrum. Meth. 119 (1974) 157.

[11] CMS Collaboration, Precise determination of the mass of the higgs boson and studies of the compatibility of its couplings with the standard model, CMS-PAS-HIG-14-009.